Nanoscale

PAPER

View Article Online
View Journal | View Issue

Cite this: *Nanoscale*, 2024, **16**, 7093

Discarding metal incorporation in pyrazole macrocycles and the role of the substrate on single-layer assemblies†

Jorge Lobo-Checa, *[a,b,c] Sindy Julieth Rodríguez, [d] Leyre Hernández-López, [a,b] Lucía Herrer, [a,c] Mario C. G. Passeggi, Jr., [d,e] Pilar Cea [a,c,f] and José Luis Serrano *[a,g]

Pyrazole derivatives are key in crystal engineering and liquid crystal fields and thrive in agriculture, pharmaceutical, or biomedicine industries. Such versatility relies in their supramolecular bond adaptability when forming hydrogen bonds or metal-pyrazole complexes. Interestingly, the precise structure of pyrazole-based macrocycles forming widespread porous structures is still unsolved. We bring insight into such fundamental question by studying the self-assembled structures of a bis-pyrazole derivative sublimed in ultra-high-vacuum conditions (without solvents) onto the three (111) noble metal surfaces. By means of high-resolution scanning tunneling microscopy that is validated by gas phase density functional theory calculations, we find a common hexagonal nanoporous network condensed by triple hydrogen bonds at the molecule–metal interface. Such assembly is disrupted and divergent after annealing: (i) on copper, the molecular integrity is compromised leading to structural chaos, (ii) on silver, an incommensurate new oblique structure requiring molecular deprotonation is found and, (iii) on gold, metal–organic complexes are promoted yielding irregular chain structures. Our findings confirm the critical role of these metals on the different pyrazole nanoporous structure formation, discarding their preference for metal incorporation into the connecting nodes whenever there is no solvent involved.

Received 31st July 2023,
Accepted 12th March 2024

DOI: 10.1039/d3nr03773h

rsc.li/nanoscale

Introduction

The structure of pyrazole (Fig. 1a) is widespread in many science fields with derivatives involved in applications as diverse as biomedicine, environmental or materials science, metallurgy *etc.*[1–6] Such prevalence relies on the versatility of the pyrazole ring to generate different intermolecular interactions that drives the overall structure of the complexes. Particularly, the molecular adaptability brought by a lone, basic nitrogen and an adjacent N–H group that combines into

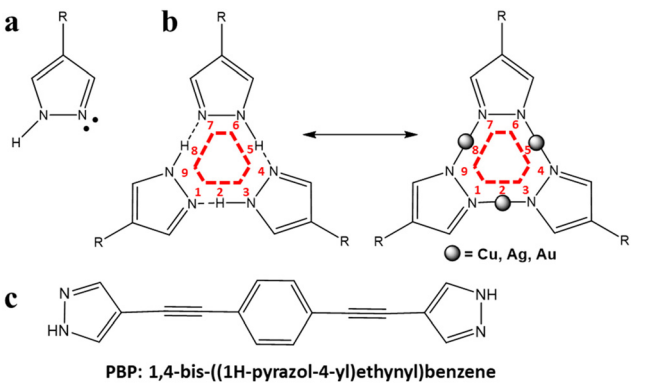

Fig. 1 (a) The pyrazole moiety and (b) the two possible cases for the nine-member (9-atom) macrocycles conformations (the atoms are numbered around the discontinuous red line). It is unclear whether metals are incorporated after a triple deprotonation. (c) Double linear pyrazole derivative (**PBP**) used in this work. Note that the linear linkers allow for rotation and torsion of the pyrazole groups with respect to the central phenyl group.

[a]*Instituto de Nanociencia y Materiales de Aragón (INMA), CSIC-Universidad de Zaragoza, Zaragoza 50009, Spain. E-mail: jorge.lobo@csic.es, joseluis@unizar.es*
[b]*Departamento de Física de la Materia Condensada, Universidad de Zaragoza, E-50009 Zaragoza, Spain*
[c]*Laboratorio de Microscopias Avanzadas, Universidad de Zaragoza, E-50018 Zaragoza, Spain*
[d]*Instituto de Física del Litoral, Consejo Nacional de Investigaciones Científicas y Técnicas y Universidad Nacional del Litoral (IFIS-Litoral, CONICET-UNL), Santa Fe, Argentina*
[e]*Departamento de Física, Facultad de Ingeniería Química, Universidad Nacional del Litoral, Santa Fe, Argentina*
[f]*Departamento de Química Física, Facultad de Ciencias, Universidad de Zaragoza, E-50009 Zaragoza, Spain*
[g]*Departamento de Química Orgánica, Facultad de Ciencias, Universidad de Zaragoza, E-50009 Zaragoza, Spain*
† Electronic supplementary information (ESI) available. See DOI: https://doi.org/10.1039/d3nr03773h

strong H-bonds, together with the ring aromaticity, are key in the formation of supramolecular organizations. Among others, linear polymeric structures, flat discoid complexes formed by dimers, trimers, tetramers, *etc*. or three-dimensional arrangements based on interactions between pyrazole derivatives through hydrogen bonds have been described.[7–11] Additionally, interesting properties like gel and liquid crystal behavior, luminescence or materials for energy storage have been reported within such kind of supramolecular organizations.[12–14]

The pyrazole-based structures and geometries are manifold expanded whenever mixed with metals. As bonding options increase, they incorporate covalent bonds or ionic interactions, which yield highly-stable structures.[15–20] Notably, rod- or disc-like metal complexes of pyrazole derivatives can lead to liquid crystal properties as they present a high number of terminal chains that favor intermolecular interactions. Aside from the weaker interactions between organic moieties leading to the liquid crystal state, the metallophilic interactions can play a critical role in the final structures.[21–24] This is noteworthy in the case of trimeric nine-membered macrocyclic complexes formed with Cu, Ag and Au, where in addition to multichain structures,[25–29] mesophases with only three short terminal chains were reported.[30] Such structures closely resemble those formed by three supramolecular H-bond pyrazole molecules (see Fig. 1b),[10,11] but leave open whether the hydrogens are replaced by metal centers in these macrocycles in the absence of solvents.

To shed light into the pyrazole interactions we designed an experiment where a pyrazole derivative is deposited in ultra-high-vacuum (UHV, without solvents) onto the (111) surface planes of the three noble metals (Cu, Ag and Au), as conducted for other molecular precursors.[31–34] By inspecting their arrangements using high-resolution scanning tunneling microscopy (STM) and corroborating them by means of gas-phase (free standing) density functional theory (DFT) calculations, we first demonstrate that an elementary hexagonal structure is formed onto these three surfaces. Then we subject them to an equivalent thermal treatment to promote catalytic reactions that could trigger deprotonation, which could lead to the creation of metallophilic complexes (metal-pyrazole interactions) by Cu, Ag or Au intercalation. The molecule chosen for this study is a double linear pyrazole derivative (**PBP**). This molecule is shown in Fig. 1c and has been described as a generator of linear and porous supramolecular structures.[35] Notably, it is an extraordinary one-dimensional conductor, where the pyrazole moiety is attached in face or end geometries with the gold contacts.[36] Indeed, the pyrazole heterocycles are identified as excellent anchor groups capable of forming well-ordered Langmuir–Blodgett monolayers on gold substrates.[37] However, the in-solution self-assembly of films of **PBP** on gold, where the axis of the molecule stays almost perpendicular to the surface, turn out to be irregular given the significant atom extraction from the substrate after the time of immersion in the solvent. This evidences the relevant interaction strength between the Au substrate and the pyrazole fractions of the **PBP**. Therefore, if energetically favorable, the formation of metallophilic complexes should be detectable.[38–40]

Results

Room temperature assemblies of PBP on the three noble metal surfaces

Sub-monolayer deposition of **PBP** on the three noble metal surfaces at room temperature (RT) in UHV conditions lead to planar molecular adsorption (Fig. 2). Independently of the interaction with the substrate, which should be largest for Cu (111) and weakest for Au(111),[41,42] the phenyl and pyrazole groups are parallel to the three surfaces. Such adsorption maximizes the π-ring interaction with the metal substrate, which imposes lateral-end group interactions on the self-assembled arrangements. Indeed, the hexagonal porous arrangement is stabilized by trimeric structures linked through N–H···N bonds on the three substrates, as shown in Fig. 3. These intermolecular interactions result in a nine-membered (9-atom) supramolecular macrocycle that leaves no space for metal complexes. Such finding evidences the stability of the pyrazole H-bonds compared to the existing molecular interactions with the underlying noble metal surfaces.[43–45]

A careful inspection of Fig. 2 shows that the central phenyl group of each **PBP** is imaged brighter and wider than the outer pyrazole rings. Moreover, the hexagonal pores exhibit a certain irregularity, which stems from the flexibility of the linear linkers connecting the benzene ring with the pyrazole groups. In consequence, the molecules can sit in different atomic rows and introduce slight deviations from the three main high-symmetry directions of these substrates. Additionally, we identify rotational domains in these images. In the case of Cu(111), the stronger interaction of **PBP** with the substrate results in rather small islands with different relative orientations. Contrarily, extended single domains were found in the case of Ag(111) despite the general pore deformation observed. This indicates that the intermolecular interaction dominates (but not totally) over the substrate-molecule one, allowing distant molecular diffusion over the surface that can then aggregate into extended domains.

The case of **PBP** on Au(111) is not as straightforward as on Cu(111) and Ag(111). On the one hand, the hexagonal network is quite regular in several visible patches of Fig. 2c, but on the other hand, disordered linear oligomeric (spaghetti-like) chains on the surface are found. Fig. S1† shows high-resolution images of such disordered chains, evidencing that metal-organic bond formation is at their origin. We find that Au adatoms become attached to the external rings of **PBP** molecules. The most possible source of these Au adatoms originate from step-edges since they exhibit irregular shapes after **PBP** deposition. Importantly, triple H-bonds leading to the 9-member rings are still visible in these disordered regions reminiscent from the hexagonal assembly without metal coordination.

The stability of this 9-member macrocycle is theoretically checked by performing first-principles calculations based on

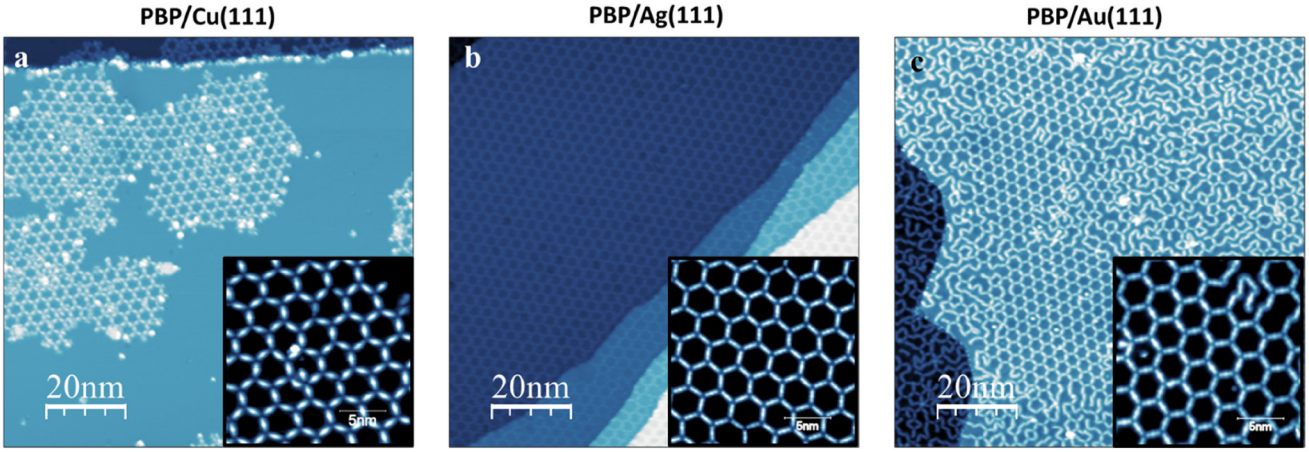

Fig. 2 STM images at 5 K of **PBP** deposited on the three (111) noble metal surfaces kept at RT. A common hydrogen bonded hexagonal network is self-assembled on the three surfaces. Note that networks are not precisely regular and show different rotational domains. Exceptionally for Au(111), metal–organic bonding exists yielding disordered chain-like structures, which coexist with the hexagonal networks. STM acquisition details: (a) overview 100 × 100 nm^2, −0.5 V, 100 pA; inset: 20 × 20 nm^2, 0.100 V, 130 pA; (b) overview 100 × 100 nm^2, 0.01 V, 130 pA; inset: 20 × 20 nm^2, −0.010 V, 130 pA; (c) overview 100 × 100 nm^2, −1.0 V, 100 pA; inset: 20 × 20 nm^2, −0.100 V, 100 pA.

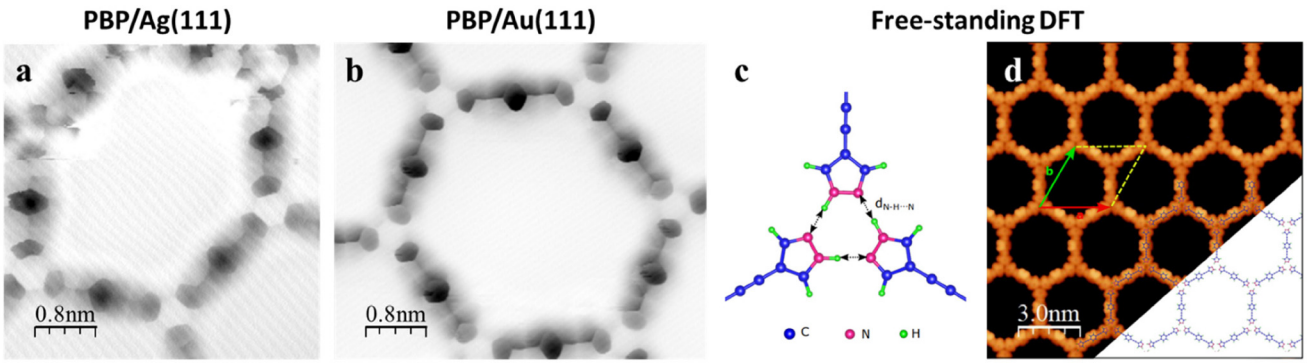

Fig. 3 Bond-resolved STM images acquired at constant height mode with a functionalized CO tip of **PBP** on (a) Ag(111) and (b) Au(111). In these images the central phenyl rings appear darker than the pyrazole rings, which exhibit a separation of the order of 0.25 ± 0.03 nm. As the position of the hydrogen atoms are not imaged, we assume the theoretical separation of the covalent N–H bond (0.10 nm) to estimate the experimental hydrogen bond distance $d^{exp}_{N-H\cdots N}$ = 0.25–0.10 = 0.15 ± 0.03 nm. (c) Gas phase (free-standing) DFT calculations showing that the most stable hexagonal configuration is planar forming a nine-membered (9-atom) ring that are stabilized *via* triple N–H···N bonds (without metal incorporation). The resulting bond distance is $d_{N-H\cdots N}$ = 0.188 nm. (d) Simulated STM image of a regular, free-standing hexagonal network, which agrees with the insets of Fig. 2. STM bond-resolved image details: (a) 4.2 × 4.2 nm^2, −0.16 mV (STM bias offset); (b) 4.2 × 4.9 nm^2, −0.16 mV (STM bias offset). DFT simulations image details in (d): 15 × 15 nm^2, V_b = 1 V.

density functional theory (DFT) in the gas phase (without substrate, see the Materials and Methods section in the ESI†). We start by relaxing the **PBP** molecule to remove the internal stress and then construct the hexagonal arrangement by including three molecules per unit cell (90 atom calculation). After fully relaxing the system (both lattice parameters and atomic positions), we reproduce the experimental arrangement of the pyrazole groups forming a 9-member ring. In essence, the molecules adopt practically a linear configuration with planar bonding geometry without metal adatoms to coordinate. The hydrogen bond results in an average distance of $d_{N-H\cdots N}$ = 0.188 nm (Fig. 3c), which agrees with the average values reported for similar pyrazole trimers.[46–48] This value is slightly larger than the estimated experimental distance of 0.15 ± 0.03 nm (see caption of Fig. 3) that we attribute to a substrate induced compression together with the arching of the molecular backbone. Importantly, with this calculated geometry in the gas phase, the simulated STM image in Fig. 3d matches convincingly the three experimental hexagonal arrangements.

We can evaluate the molecule-substrate interaction by comparing this gas phase calculations with the ones found experimentally on each surface. To this end, we extract the periodicity of the hexagonal network on the three surfaces using the self-correlation function and the pore area, which are summarized in Table 1. From this analysis we find that the hexagonal network on Ag(111) exhibits the shortest average periodicity and the smallest pore area, but has the largest spread in the

Table 1 Average periodicities of the hexagonal arrangement on the three noble metal surfaces obtained using the self-correlation function on several STM images of lateral sizes of the order of 25 nm (processing over than 100 pores per surface). Their spread from the average value is checked extracting the longest, middle and shortest axis (columns 2 to 4), where the number in parentheses indicates how much it differs from the average periodicity (column 5). The last column estimates the pore size considering their average periodicity and subtracting the estimated molecular width (0.7 nm)

	Longer axis (nm)	Mid axis (nm)	Shorter axis (nm)	Periodicity (nm)	Pore area (nm^2)
Hexagonal **PBP** on Cu(111)	3.54 (0.06)	3.50 (0.02)	3.39 (−0.09)	3.48	6.69
Hexagonal **PBP** on Ag(111)	3.37 (0.10)	3.25 (−0.02)	3.19 (−0.08)	3.27	5.72
Hexagonal **PBP** on Au(111)	3.37 (0.02)	3.35 (0.00)	3.33 (−0.02)	3.35	6.09

three axis. This arrangement on Cu(111) has practically the same spread, but exhibits the longest periodicity and pore size of the three noble metal surfaces. Contrarily, on Au(111) the axial spread is practically nonexistent, so this network appears to be less influenced by the substrate. Indeed, it is the network on Au the one that best matches with the DFT gas phase calculations (3.37 nm and 6.17 nm^2). This comes to show that the molecule-substrate interaction on Au is smallest of the three noble metal surfaces, in agreement with previous work.[31–34]

Annealing treatment of the PBP networks on the three substrates

To challenge the stability of the triple H-bonds that promote the formation of hexagonal macrocycles on the three transition metals, the samples were mildly annealed up to approximately 90 °C. Such temperature could possibly induce the formation of metallophilic complexes, where deprotonation would allow metal adatoms to replace the H atoms (see Fig. 1b) thereby leading to higher supramolecular organizations. Indeed, we find that after this treatment the molecular interactions are redefined given the enhanced **PBP** mobility and the increment of adatoms diffusing over the surface. Nevertheless, the different substrate-molecule interactions lead to divergent scenarios after this annealing process, as shown in Fig. 4. The high-temperature (HT) annealed **PBP** on Cu(111) produces highly amorphous structures without any discernible periodicity (Fig. 4a). A close inspection of the STM images shows that the individual molecules (imaged before as elongated features broadened at the center) are compromised. Indeed, recognizable **PBP** coexist with molecular fragments and products resulting from uncontrolled molecular reactions, which suggests that the **PBP** integrity is strongly affected on Cu(111) at these temperatures. This fragmentation is similar to that previously observed for the cleavage of the bond C(sp)–C(sp^3) assisted by copper adatoms,[49] which on this surface would detach the pyrazole group from the closest alkyne carbon ($C_{pyrazol}$-/-C_{alkyne}). Note that such molecular fracture is absent at this temperature on the other two noble metal surfaces (see Fig. 4b and c), which is justified by their comparatively lower catalytic reactivity compared to Cu(111).[50,51]

Nonetheless, stark differences between the high temperature arrangements on Ag and Au are evidenced. In the case of Ag(111), we find that the hexagonal network is practically replaced by a highly regular oblique structure (*cf.* Fig. 4b and S2†). Note that this new arrangement is absent if annealed at lower temperatures (*e.g.* at ∼75 °C), where we find instead an improved and highly extended hexagonal network (see Fig. S3a and b†). This oblique structure has molecules aligning at two different directions forming an angle of approximately 105°. In the first direction, the linear axis of the **PBP**s practically line up (dashed green line), whereas in the other direction (dashed yellow line) these adopt a staggered arrangement. Each node of the lattice consists of four pyrazole units, as evidenced in Fig. 5a and b. Notably, some pyrazole groups are no longer symmetric along the non-staggered direction (discontinuous green lines in Fig. 5a), which we attribute to rotations of these with respect to the phenyl groups. The positions of these rotated pyrazole units are indicated by green and red points that we find in alternating rows (*cf.* green and red arrows in the top of Fig. 5a).

Given the complexity of this oblique network, we performed gas-phase DFT calculations to model this assembly. The experimentally detected pyrazole rotations require that the supercell contains two oblique subunits, defined by the parallelogram enclosed by the dashed yellow lines in Fig. 5. In agreement with the experiment, the constituent molecules of the most stable configuration exhibit an alignment along two preferential directions forming an angle of 103.9°, one of them adopting a staggered configuration (see the simulated STM image in Fig. 5c). At the connecting nodes, four pyrazole rings interact, three of them forming a quasi-planar 9-member ring reminiscent of the hexagonal arrangement. Remarkably, one of the three accomplishes the hydrogen bond replacing the N–H···N bond by C–H···N, which introduces the change in angle in the staggered direction. Note that this 9-member ring is not equilateral (as in the case of the hexagonal arrangement), but is isosceles since the average distance of the N···H–N hydrogen bonds is shorter than the N···H–C one (0.187 nm *vs.* 0.240 nm). Such increased separation implies a weaker interaction of the N···H–C bond with respect to the N···H–N bond, so that slight rotations of the pyrazole groups become possible. The connection to the fourth molecule is more complex, as we find that its pyrazole requires to be deprotonated. Contrarily, constructing this arrangement with non-deprotonated **PBP** molecules results in evident disagreement with the experimental findings related to the rotation of the pyrazole groups external to the 9-member rings that introduces more irregularity into the calculated arrangement (see Fig. S4†). The deprotonated pyrazole rotates away by almost 36.5° due to the repulsive nature of the N–H···H–C interaction,

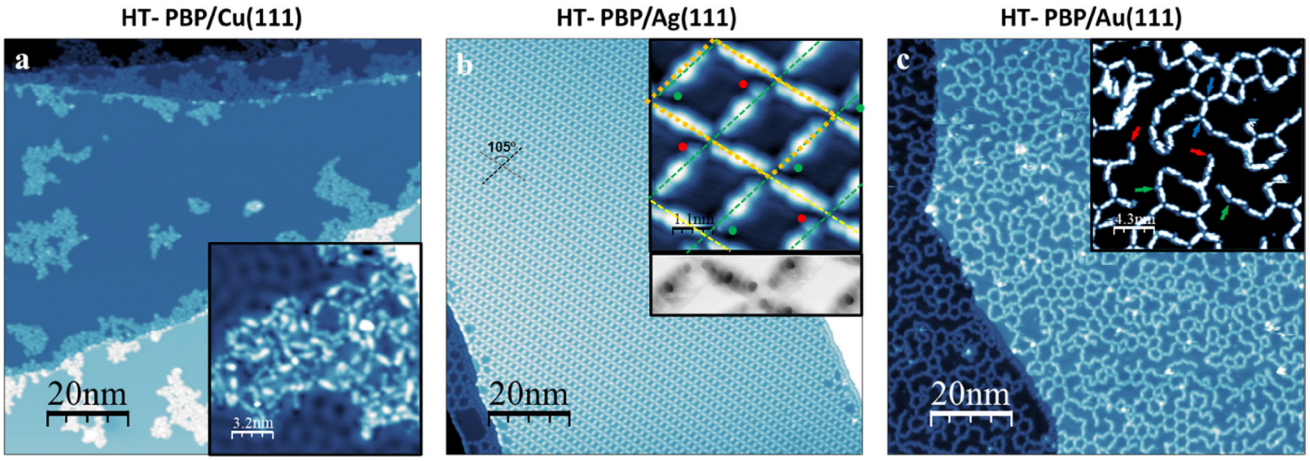

Fig. 4 STM images of **PBP** on the three (111) noble metal surfaces after annealing to 90 °C. (a) For **PBP** on Cu(111) the annealing process induces the rupture and uncontrolled reactions of the molecules preventing ordered structures. (b) In the case of Ag(111) a new oblique arrangement coexists with a residual amount of the hexagonal network. The average molecular directions (angle of ~105°) do no longer follow the high-symmetry substrate directions. In the inset we observe different intensities of the **PBP** depending on their orientation, finding stronger variations along the green lines, especially at the pyrazole groups marked by green or red points. Only a small portion of this network could be measured in the bond-resolved constant height mode imaging before the tip was strongly modified (bottom inset). (c) For **PBP** annealed on Au(111) the hexagonal network is replaced by disordered metalorganic chains. Note that Au adatoms are found within the chains (green arrows) and at chain terminations (red arrows), but are absent at the triple H-bond macrocycles (dim blue arrows). STM image details: (a) overview 100 × 100 nm^2, 1.0 V, 130 pA; inset: 16 × 16 nm^2, 0.01 V, 130 pA; (b) overview 100 × 100 nm^2, 1.0 V, 130 pA; inset top: 5.4 × 5.4 nm^2, 0.01 V, 50 pA; inset bottom: 5.4 × 1.5 nm^2, −0.16 mV (STM bias offset), acquired with a CO functionalized tip in constant height mode; (c) overview 100 × 100 nm^2, 1.0 V, 100 pA; inset: 21.5 × 21.5 nm^2, 0.01 V, 30 pA, acquired with a CO funcionalized tip.

causing the hydrogen atom to move away from the 9-member ring plane (see Fig. 5d). In this way, the calculated distance between neighboring hydrogens increases up to 0.267 nm, which is significantly larger than the in-plane projection (0.187 nm without rotation).

This modified pyrazole (rotated and deprotonated) in combination with the substrate must necessarily improve the stability of the system, since the oblique arrangement completely replaces the hexagonal structure. We expect a mechanism where the deprotonated C efficiently binds to the underlying Ag atoms of the surface, but this can only be validated with calculations that include the Ag substrate. At the opposite side of this modified pyrazole, the interaction of the STM tip becomes significant in comparison with the rest of the network due to its protrusion away from the substrate. This is especially evident when acquiring bond-resolved images by functionalized CO tips in constant height mode, since the full unit cell could never be completed (see bottom inset of Fig. 4b) and in constant current mode tiny circular blobs are detected (Fig. 5a and b).

Moving on to the case of high-temperature annealing of **PBP** on Au(111), we find in Fig. 4c that the hexagonal arrangement has practically vanished. Heating up the substrate increases the number of metal atoms available on the terraces, which should stimulate the metalorganic bond formation. Indeed, linear oligomers stabilized by Au centers (visible as circular features as indicated by red and green arrows in the inset) now dominate on the surface. The substitution of the triple N–H···N bonds stabilizing the hexagonal structure for disordered metalorganic chains turns out to be progressive with temperature. This is clear from the inspection of the intermediate case presented in Fig. S3c and d,† which is roughly halfway between the cases shown at RT (Fig. 1c) and HT (Fig. 4c). This gradual change can be qualitatively understood from two complementary effects: on the one hand, the higher temperature efficiently dissociates the H-bonds and liberates molecules to diffuse over the surface and, on the other, the amount of available Au adatoms on the surface increases with temperature. As a result, free molecules have a higher probability of finding an Au atom and consolidate a metalorganic bond at the lone nitrogen atoms of the pyrazoles. According to these images, once the metal–organic bond has been generated it is unfavourable to replace it by an H-bond, evidencing the greater strength of the metal–organic bond with Au. Such effect supports the reported extraction of atoms from the surface after incubation of the gold substrate in a **PBP** solution.[37]

Discussion

The absence of solvents and residual gases in UHV induces a planar configuration of the molecules on the surface, where the usual π–π stacking is replaced by planar adsorption of **PBP**s on the noble metal surfaces seeking their higher electronic density.[38–40,43,44,50] This restricts the intermolecular interactions to the plane thereby promoting the N···H bonds between the pyrazole moieties. Consequently, the molecules

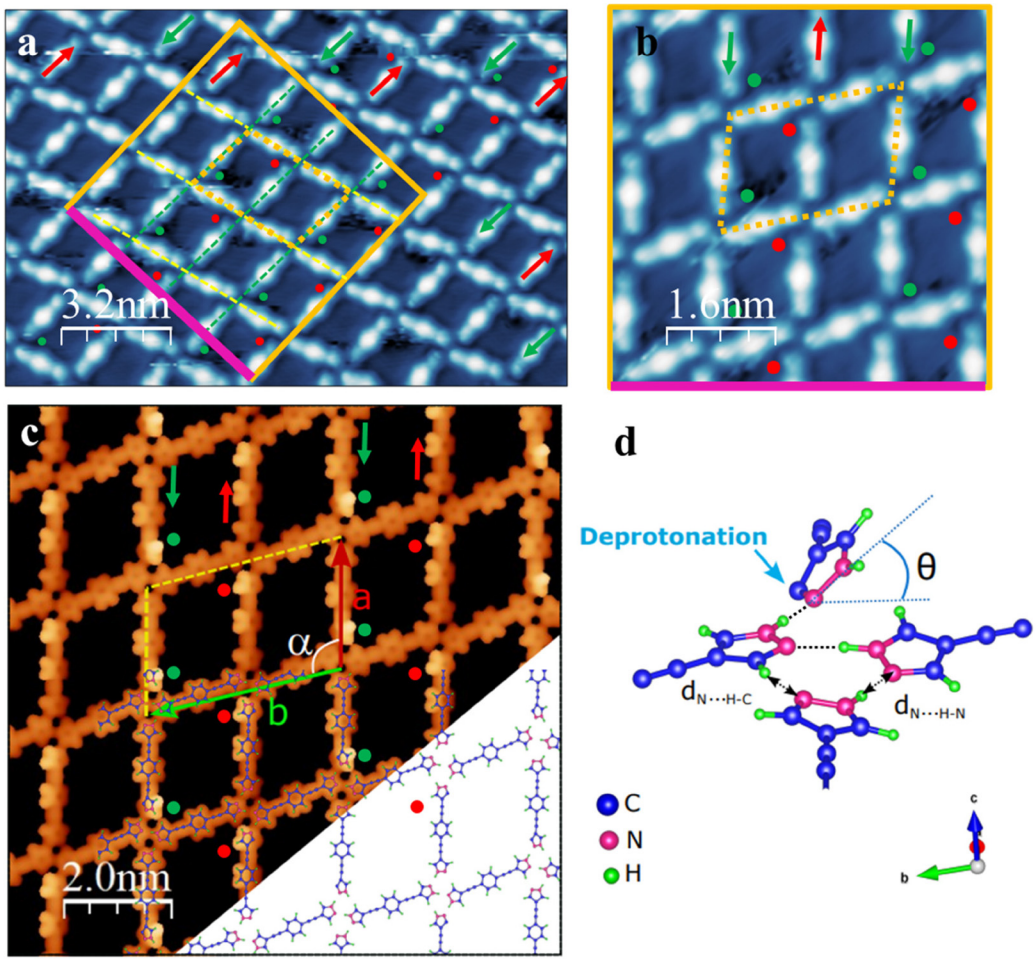

Fig. 5 (a) High-resolution STM image and (b) its anti-clockwise rotated close up of the high temperature oblique arrangement of **PBP** on Ag(111). The green and red points at the side of pyrazole groups indicate intensity differences, which we attribute to pyrazole rotations. These pyrazole rotations alternate in the molecular lines, as marked by green and red arrows on the top of image (a). Note the tiny blobs in some of the rotated pyrazole groups, which are likely outward protruding hydrogens, and also the horizontal streaks caused by the CO molecule movements at the tip apex when interacting with other adsorbed CO molecules at the pores. (c) Simulated STM image obtained from gas phase DFT calculations. To account for the pyrazole rotations, the supercell required is the one enclosed by the yellow dashed lines, which exhibits an exceptional agreement with the experimental data. (d) Model of a node of the oblique arrangement that consists of two N···H–N bonds and one C–H···N bond forming an almost planar nine membered (9-atom) ring, which coexists with a rotated pyrazole of the fourth molecule. The latter interacts through a N–H···N bond that is only feasible after deprotonation of the carbon contiguous to the pyridine-like nitrogen of the pyrazole ring. In presence of a substrate, we infer that such deprotonation and rotation would enable a C···Ag interaction with the substrate. STM image details: (a) 16 × 10.7 nm^2 ((b) 8.0 × 5.4 nm^2), 0.01 V, 30 pA (functionalized CO tip). (c) DFT simulated STM image: 10 × 10 nm^2, V_b = 1 V.

form hexagonal networks at RT built by nine-member (9-atom) macrocycles on the three substrates studied. However, the molecule-substrate interaction is different on these three noble metal surfaces, as extracted from the different periodicities (see Table 1). Indeed, on Au(111) the periodicity of the hexagonal network practically matches the DFT gas phase values, implying a relatively weak molecule-substrate interaction. In comparison, this same network formed on Ag is found to be contracted by 2.4%, whereas on Cu it is expanded by 3.9%. Nevertheless, judging from the small relative size of the domains found on Cu(111) compared to Ag(111), the molecule-surface interaction must be the strongest for the former, in agreement to other molecular precursors.[31–34] Importantly, on the hexagonal network metal adatoms were never detected experimentally nor justified theoretically, which excludes metallophilic complexes formation on these surfaces in UHV. This implies that (without solvent) the metal substitution is here unfavorable (see Fig. 1b).[25–30]

The only exception to N···H–N bond formation at RT is the metalorganic bond of the **PBP**s with Au adatoms. This could have been anticipated from the pyrazole affinity to Au atoms compared to Ag or Cu, as reported when forming self-assembled layers of **PBP** on gold in solution.[37,51] Even without solvent, we find in UHV a severe roughening of the substrate step-edges that we associate to this pyrazole-Au strong bonding, which is absent on Ag or Cu (*cf.* Fig. 2, 4 and S3†).

This metalorganic bond is stimulated when increasing the temperature, leading to adatom detection even at the chain terminations (red arrows in inset of Fig. 4c).

Finally, the oblique arrangement observed on Ag(111) that can only be stabilized at the highest temperatures deserves further attention. Evidently, the pyrazole (and phenyl) rotations are energetically unfavorable, so the new C–H···N bonds at the nodes seem insufficient to condensate this new arrangement. Based on our DFT calculations and the high temperature onset experimentally determined (close to ~90 °C), the on-surface reaction leading to the pyrazole deprotonation is the only plausible explanation we can find for the stability of this oblique arrangement. Although more complex calculations that include the underlying substrate are necessary to verify this, we infer that the radical formation must be compensated by the high gain when the pyrazole becomes bound to the underlying Ag atoms of the terrace. This explains the strong quenching in intensity observed at the island terminations (under-coordinated positions) in Fig. S2a and b,† which concurs with a severe charge depletion due to the binding of the rotated pyrazole with the Ag substrate.

Conclusions

By high-resolution STM and DFT calculations in the gas-phase we study the self-assembled structures of a double linear pyrazole derivative on the three (111) noble metal surfaces in UHV without the use of solvents. After deposition at room temperature, we find a common hexagonal arrangement on all surfaces and determine the precise structure of the pyrazole-based macrocycles. Importantly, we find no trace of metal substitution of the triple H-bonds in this 9-member rings. Remarkably, after annealing these systems, different arrangements are found for each surface resulting in a new oblique structure (on Ag), or promoting metal–organic chains (on Au), or destroying the integrity of the molecules (on Cu). Special attention is dedicated to the oblique arrangement since we find a selective pyrazole rotation that is generally absent on flat poly-aromatic hydrocarbon systems, which is accompanied by a deprotonation of this group. Interestingly, the 9-member ring found at room temperature prevails, but one of the N–H···N bonds is replaced by a C–H···N one. In essence, we determine that the role of the metal substrate and their adatoms is critical on the final structure formation.

Author contributions

J. L.-C. and L. H.-L. conducted the experiment and its data analysis; L. H., P. C. and J. L. S. designed, synthesized and purified the **PBP** compound; S. J. R. performed the computational calculations; J. L.-C. and J. L. S. wrote the manuscript. All authors contributed to the revision and final discussion of the manuscript.

Conflicts of interest

The authors declare no competing financial interests.

Acknowledgements

We gratefully acknowledge financial support from the Spanish Ministries of Economy, Industry and Competitiveness (MINECO, grants MAT2016-78293-C6-4-R and MAT2016-78293-C6-6) and of Science and Innovation (MICINN, grant PID2019-107338RBC64, PID2019-105881RB-I00, PID2021-122882NB-I00, PID2022-141433OB-I00 and PID2022_138750NB-C21/AEI/10.13039/501100011033 and RED2018-102833-T) including the Spanish Research Agency (AEI) and the European Regional Development Fund (ERDF), from the regional Governments of Aragon (E12_23R, E47_23R and E31_23R) and from the European Commission through the project ULTIMATE-I, grant ID 101007825. The present work used computational resources of the Pirayu cluster, acquired with funds from the Santa Fe Science, Technology and Innovation Agency (ASACTEI), Government of the Province of Santa Fe, through Project AC-00010-18, resolution no. 117/14.

References

1 J. Xu, H. B. Tan, Y. J. Zhang, *et al.*, Catalyst-Free One-Pot Synthesis of Densely Substituted Pyrazole-Pyrazines as Anti-Colorectal Cancer Agents, *Sci. Rep.*, 2020, **10**, 9281, DOI: 10.1038/s41598-020-66137-z.

2 K. Karrouche, S. Radi, Y. Ramli, J. Taoufik, Y. N. Mabkhot, F. A. Al Aizari and M. Ansar, Synthesis and Pharmacological Activities of Pyrazole Derivatives: A Review, *Molecules*, 2018, **23**, 134, DOI: 10.3390/molecules23010134.

3 H. Song, Y. Liu, L. Xiong, Y. Li, N. Yang and Q. Wang, Design, Synthesis, and Insecticidal Evaluation of New Pyrazole Derivatives Containing Imine, Oxime Ether, Oxime Ester, and Dihydroisoxazoline Groups Based on the Inhibitor Binding Pocket of Respiratory Complex I, *J. Agric. Food Chem.*, 2013, **61**, 8730–8736.

4 S. Tighadouini, S. Radi, M. El Massaoudi, Z. Lakbaibi, M. Ferbinteanu and Y. Garcia, Efficient and Environmentally Friendly Adsorbent Based on β Ketoenol-Pyrazole-Thiophene for Heavy-Metal Ion Removal from Aquatic Medium: A Combined Experimental and Theoretical Study, *ACS Omega*, 2020, **5**, 17324–17336.

5 A. Tigreros and J. Portilla, Recent progress in chemosensors based on pyrazole derivatives, *RSC Adv.*, 2020, **10**, 19693–19712.

6 A. Harbindu, *et al.*, *Water-soluble pyrazole derivatives as corrosion inhibitors. International application published under the patent cooperation treaty (PCT)*, WO 2016/191677 A1 and PCT/US2016/034635, 2016.

7 S. Millan, J. Nasir, B. Gil-Hernández, T.-O. R. Knedel, B. Moll, I. Boldog, O. Weingart, J. Schmedt auf der Günne

and C. Janiak, Solid-State Landscape of 4,4′-Azobis(3,5-dimethyl-1H-pyrazole) with the Isolation of Conformer-Dependent Polymorphs, *Cryst. Growth Des.*, 2020, **20**, 2721–2733.

8 W.-X. Liu, Z. Yang, Z. Qiao, L. Zhang, N. Zhao, S. Luo and J. Xu, Dynamic multiphase semi-crystalline polymers based on thermally reversible pyrazole-urea bonds, *Nat. Commun.*, 2019, **10**, 4753, DOI: 10.1038/s41467-019-12766-6.

9 S. Radi, M. El-Massaoudi, H. Benaissa, N. N. Adarsh, M. Ferbinteanu, E. Devlin, Y. Sanakis and Y. Garcia, Crystal engineering of a series of complexes and coordination polymers based on H-bonds pyrazole-carboxylic acid ligands, *New J. Chem.*, 2017, **41**, 8232.

10 U. P. Singh, K. Tomar and S. Kashyap, Supramolecular assemblies of benzene-1,3,5-tricarboxylic acid and 3,5-substituted pyrazoles:formation and structural analysis, *CrystEngComm*, 2015, **17**, 1421.

11 C. Foces-Foces, A. Echevarría, N. Jagerovic, I. Alkorta, J. Elguero, U. Langer, O. Klein, M. Minguet-Bonvehı and H. H. Limbach, A Solid-State NMR, X-ray Diffraction, and ab Initio Computational Study of Hydrogen-Bond Structure and Dynamics of Pyrazole-4-Carboxylic Acid Chains, *J. Am. Chem. Soc.*, 2001, **123**, 7898–7906.

12 I. Gospodinov, K. V. Domasevitch, C. C. Unger, T. M. Klapötke and J. Stierstorfer, Midway between Energetic Molecular Crystals and High-Density Energetic Salts: Crystal Engineering with Hydrogen Bonded Chains of Polynitro Bipyrazoles, *Cryst. Growth Des.*, 2020, **20**, 755–764.

13 S. Moyano, J. Barberá, B. E. Diosdado, J. L. Serrano, A. Elduque and R. Giménez, Self-assembly of 4-aryl-1H-pyrazoles as a novel platform for luminescent supramolecular columnar liquid crystals, *J. Mater. Chem. C*, 2013, **1**, 3119–3128.

14 S. Moyano, J. L. Serrano, A. Elduque and R. Giménez, Self-assembly and luminescence of pyrazole supergelators, *Soft Matter*, 2012, **8**, 6799.

15 A. Oulmidi, S. Radi, H. N. Miras, N. N. Adarsh and Y. García, New. Bis-Pyrazole-Bis-Acetate Based Coordination Complexes: Influence of Counter-Anions and Metal Ions on the Supramolecular Structures, *Sustainability*, 2021, **13**, 288, DOI: 10.3390/su13010288.

16 U. P. Singh, S. Kashyap, H. J. Singh and R. J. Butcher, Anion directed supramolecular architecture of pyrazole based ionic salts, *CrystEngComm*, 2011, **13**, 4110.

17 S. Yuan, L. Feng, K. Wang, J. Pang, M. Bosch, C. Lollar, Y. Sun, J. Qin, X. Yang, P. Zhang, Q. Wang, L. Zou, Y. Zhang, L. Zhang, Y. Fang, J. Li and H.-C. Zhou, Stable Metal–Organic Frameworks: Design, Synthesis, and Applications, *Adv. Mater.*, 2018, **30**, 1704303.

18 A. W. Brown, Chapter Two - Recent Developments in the Chemistry of Pyrazoles, in *Advances in Heterocyclic Chemistry*, 2018, vol. 126, pp. 55–107.

19 J. Pérez and L. Riera, Pyrazole Complexes and Supramolecular Chemistry, *Eur. J. Inorg. Chem.*, 2009, **13**, 4913–4925.

20 T. Mochida, F. Shimizu, H. Shimizu, K. Okazawa, F. Sato and D. Kuwahara, Ferrocenylpyrazole—A versatile building block for hydrogen-bonded organometallic supramolecular assemblies, *J. Organomet. Chem.*, 2007, **692**, 1834–1844.

21 L. Soria, M. Cano, J. A. Campo, M. R. Torres and C. Lodeiro, Silver compounds based on N,N,N-tridentate pyridylpyrazolate ligands. An opportunity to build cyclic trimetallic and oligomeric luminescent liquid crystals, *Polyhedron*, 2017, **125**, 141–150.

22 E. Cavero, S. Uriel, P. Romero, J. L. Serrano and R. Giménez, Tetrahedral Zinc Complexes with Liquid Crystalline and Luminescent Properties: Interplay between Non-Conventional Molecular Shapes and Supramolecular Mesomorphic Order, *J. Am. Chem. Soc.*, 2007, **129**, 11608–11618.

23 P. Ovejero, M. J. Mayoral, M. Cano and M. C. Lagunas, Luminescence of neutral and ionic gold(I) complexes containing pyrazole or pyrazolate-type ligands, *J. Organomet. Chem.*, 2007, **692**, 1690–1697.

24 R. Giménez, A. Elduque, J. A. López, J. Barberá, E. Cavero, I. Lantero, L. A. Oro and J. L. Serrano, Supramolecular structures and columnar mesophase induction in nondiscoid pyrazoles by complexation to rhodium(I), *Inorg. Chem.*, 2006, **45**, 10363–10370.

25 E. Beltrán, J. Barberá, J. L. Serrano, A. Elduque and R. Giménez, Chiral cyclic trinuclear gold(I) complexes with a helical columnar phase, *Eur. J. Inorg. Chem.*, 2014, 1165–1173, DOI: 10.1002/ejic.201301487.

26 H. O. Lintang, K. Kinbara, K. Tanaka, T. Yamashita and T. Aida, Self-Repair of a one-dimensional molecular assembly in mesoporous silica by a nanoscopic template effect, *Angew. Chem., Int. Ed.*, 2010, **29**, 4241–4245.

27 A. Kishimura, T. Yamashita and T. Aida, Phosphorescent organogels via "metallophilic" interactions for reversible RGB-Color switching, *J. Am. Chem. Soc.*, 2005, **127**, 179–183.

28 J. Barberá, A. Elduque, R. Giménez, F. J. Lahoz, J. A. López, L. A. Oro and J. L. Serrano, (Pyrazolato)gold complexes showing room-temperature columnar mesophases. Synthesis, properties and structural characterization, *Inorg. Chem.*, 1998, **37**, 2960–2967.

29 J. Barberá, A. Elduque, R. Giménez, L. A. Oro and J. L. Serrano, Pyrazolate golden rings: Trinuclear complexes that form columnar mesophases at room temperature, *Angew. Chem., Int. Ed. Engl.*, 1996, **35**, 2832–2835.

30 J. Cored, O. Crespo, J. L. Serrano, A. Elduque and R. Giménez, Decisive influence of the metal in multifunctional gold, silver and copper metallacycles: high quantum yield phosphorescence, color switching and liquid crystalline behavior, *Inorg. Chem.*, 2018, **57**, 12632–12640.

31 S. J. Jethwa, E. L. Kolsbjerg, S. R. Vadapoo, J. L. Cramer, L. Lammich, K. V. Gothelf, B. Hammer and T. R. Linderoth, Supramolecular Corrals on Surfaces Resulting from Aromatic Interactions of Nonplanar Triazoles, *ACS Nano*, 2017, **11**(8), 8302–8310.

32 T. Sirtl, S. Schlögl, A. Rastgoo-Lahrood, J. Jelic, S. Neogi, M. Schmittel, W. M. Heckl, K. Reuter and M. Lackinger, Control of Intermolecular Bonds by Deposition Rates at Room Temperature: Hydrogen Bonds versus Metal Coordination in Trinitrile Monolayers, *J. Am. Chem. Soc.*, 2013, **135**(2), 691–695.

33 T. A. Pham, B. V. Tran, M.-T. Nguyen and M. Stöhr, Chiral-Selective Formation of 1D Polymers Based on Ullmann-Type Coupling: The Role of the Metallic Substrate, *Small*, 2017, **13**, 1603675.

34 M. Pivetta, M.-C. Blüm, F. Patthey and W.-D. Schneider, Coverage-Dependent Self-Assembly of Rubrene Molecules on Noble Metal Surfaces Observed by Scanning Tunneling Microscopy, *ChemPhysChem*, 2010, **11**, 1558–1569.

35 S. Galli, A. Maspero, C. Giacobbe, G. Palmisano, L. Nardo, A. Comotti, I. Bassanetti, C. P. Sozzanic and N. Masciocchia, When long bis(pyrazolates) meet late transition metals: structure, stability and adsorption of metal–organic frameworks featuring large parallel channels, *J. Mater. Chem. A*, 2014, **2**, 12208–12221.

36 I. L. Herrer, A. K. Ismael, D. C. Milán, A. Vezzoli, S. Martín, A. González-Orive, I. Grace, C. Lambert, J. L. Serrano, R. J. Nichols and P. Cea, Unconventional single molecule conductance behavior for a new heterocyclic anchoring group: pyrazolyl, *J. Phys. Chem. Lett.*, 2018, **9**, 5364–5372.

37 L. Herrer, S. Martín, A. González-Orive, D. C. Milan, A. Vezzoli, R. J. Nichols, J. L. Serrano and P. Cea, pH control of conductance in a pyrazolyl Langmuir–Blodgett monolayer, *J. Mater. Chem. C*, 2021, **9**, 2882–2889.

38 L. Hernández-López, I. Piquero-Zulaica, C. A. Downing, M. Piantek, J. Fujii, D. Serrate, J. E. Ortega, F. Bartolomé and J. Lobo-Checa, Searching for kagome multi-bands and edge states in a predicted organic topological insulator, *Nanoscale*, 2021, **13**, 5216–5223.

39 B. Cirera, L. Đordevic, R. Otero, J. M. Gallego, D. Bonifazi, R. Miranda and D. Ecija, Dysprosium-carboxylate nanomeshes with tunable cavity size and assembly motif through ionic interactions, *Chem. Commun.*, 2016, **52**, 11227–11230.

40 Y.-Q. Zhang, M. Paszkiewicz, P. Du, L. Zhang, T. Lin, Z. Chen, S. Klyatskaya, M. Ruben, A. P. Seitsonen, J. V. Barth and F. Klappenberger, Complex supramolecular interfacial tessellation through convergent multi-step reaction of a dissymmetric simple organic precursor, *Nat. Chem.*, 2018, **10**, 296–304.

41 N. Koch, Energy levels at interfaces between metals and conjugated organic molecules, *J. Phys.: Condens. Matter*, 2008, **20**, 184008, DOI: **10.1088/0953-8984/20/18/184008**.

42 S. Duhm, *et al.*, PTCDA on Au(111), Ag(111) and Cu(111): correlation of interface charge transfer to bonding distance, *Org. Electron.*, 2008, **9**, 111–118, DOI: **10.1016/j.orgel.2007.10.004**.

43 Z. Yang, L. Fromm, T. Sander, J. Gebhardt, T. A. Schaub, A. Gorling, M. Kivala and S. Maier, On-surface assembly of hydrogen and halogen bonded supramolecular graphyne like networks, *Angew. Chem., Int. Ed.*, 2020, **59**, 9549–9555.

44 G. Pawin, U. Solanki, K.-Y. Kwon, K. L. Wong, X. Lin, T. Jiao and L. Bartels, A quantitative approach to hydrogen bonding at a metal surface, *J. Am. Chem. Soc.*, 2007, **129**, 12056–12057.

45 T. Steiner, The hydrogen bond in the solid state, *Angew. Chem., Int. Ed.*, 2002, **41**, 48.

46 J. P. Castaneda, G. S. Denisov, S. Y. Kecherov, V. M. Schreiber and A. V. Shurukhina, Infrared and ab initio studies of hydrogen bonding and proton transfer in the complexes formed by pyrazoles, *J. Mol. Struct.*, 2003, **660**, 25.

47 V. V. Bertolasi, P. Gilli, V. V. Ferretti, G. Gilli and C. Fernández-Castaño, Self-assembly of NH-pyrazoles via intermolecular N-H.N hydrogen bonds, *Acta Crystallogr., Sect. B: Struct. Sci.*, 1999, **55**, 985.

48 N. Tetsuya, N. Takashi and I. Takayuki, Organic kagomé lattice consisting of trimeric pyrazole and oxime supramolecular synthons from 3-pyrazolecarboxaldoxime, *CrystEngComm*, 2005, **7**, 612.

49 T. Sugiishi, A. Kimura and H. Nakamura, Copper(I)-catalyzed substitution reactions of propargylic amines: importance of C(sp)-C(sp3) bond cleavage in generation of iminium intermediates, *J. Am. Chem. Soc.*, 2010, **132**, 5332–5333.

50 T. A. Pham, F. Song, M.-T. Nguyen, Z. Li, F. Studener and M. Stöhr, Comparing Ullmann coupling on nobel metal surfaces: on-surface polymerization of 1,3,6,8-tetrabromopyrene on Cu(111) and Au(111), *Chem. – Eur. J.*, 2016, **22**, 5937.

51 E. Barrena, R. Palacios-Rivera, A. Babuji, L. Schio, M. Tormen, L. Floreano and C. Ocal, On-surface products from de-fluorination of C60F48 on Ag(111): C60, C60Fx and silver fluoride formation, *Phys. Chem. Chem. Phys.*, 2022, **24**, 2349–2356.